Reversible hydrogenation of the Zintl phases BaGe and BaSn studied by *in situ* diffraction

Henry Auer[1], Sebastian Weber[1], Thomas Christian Hansen[2], Daniel Maria Többens[3], Holger Kohlmann[1*]

[1] Institute of Inorganic Chemistry, Leipzig Universtity, Johannisallee 29, 04103 Leipzig, Germany, E-mail: holger.kohlmann@uni-leipzig.de

[2] Institut Laue-Langevin, 71 Avenue des Martyrs, CS 20156, 38042 Grenoble Cedex 9, France

[3] Helmholtz Zentrum Berlin für Materialien und Energie, Albert-Einstein-Str. 15, 12489 Berlin, Germany

Received; accepted

Keywords: Zintl phases, In situ diffraction, Neutron diffraction, Metal hydrides

Abstract. Hydrogenation products of the Zintl phases *AeTt* (*Ae* = alkaline earth; *Tt* = tetrel) exhibit hydride anions on interstitial sites as well as hydrogen covalently bound to *Tt* which leads to a reversible hydrogenation at mild conditions. *In situ* thermal analysis, synchrotron and neutron powder diffraction under hydrogen (deuterium for neutrons) pressure was applied to Ba*Tt* (*Tt* = Ge, Sn). $BaTtH_y$ ($1 < y < 1.67$, γ-phases) were formed at 5 MPa hydrogen pressure and elevated temperatures (400 - 450 K). Further heating (500 - 550 K) leads to a hydrogen release forming the new phases β-$BaGeH_{0.5}$ (*Pnma*, *a* = 1319.5(2) pm, *b* = 421.46(2) pm, *c* = 991.54(7) pm) and α-$BaSnH_{0.19}$ (*Cmcm*, *a* = 522.72(6) pm, *b* = 1293.6(2) pm, *c* = 463.97(6) pm). Upon cooling the hydrogen rich phases are reformed. Thermal decomposition of γ-$BaGeH_y$ under vacuum leads to β-$BaGeH_{0.5}$ and α-$BaGeH_{0.13}$ (*Cmcm*, *a* = 503.09(3) pm, *b* = 1221.5(2) pm, *c* = 427.38(4) pm). At 500 K the reversible reaction α-$BaGeH_{0.23}$ (vacuum) = β-$BaGeH_{0.5}$ (0.2 MPa deuterium pressure) is fast and was observed with 10 s time resolution by *in situ* neutron diffraction. The phases α-$BaTtH_y$ show a pronounced phase width (at least $0.09 < y < 0.36$). β-$BaGeH_{0.5}$ and the γ-phases appear to be line phases. The hydrogen poor (α- and β-) phases show a partial occupation of Ba_4 tetrahedra by hydride anions leading to a partial oxidation of polyanions and shortening of *Tt*-*Tt* bonds.

Introduction

Zintl phases gained some interest as reversible hydrogen storage materials since they react under mild conditions, e.g. $CaSiH_{1.3}$ [1, 2], $KSiH_3$ [3, 4] or $SrAl_2H_2$ [5, 6]. Chemisorbed hydrogen storage materials can be divided into (i) ionic (e.g. MgH_2) or (ii) complex metal hydrides (e.g. $NaAlH_4$, or $LiBH_4$) or (iii) molecular hydrides (e.g. NH_3BH_3). [7-12]. Ionic metal hydrides like MgH_2 exhibit strong Coulomb interactions of the hydride anions with metal cations and thus show high desorption temperatures. In complex metal hydrides like alanates or boronates, however, hydrogen is covalently bound to an element forming a complex anion. Unfortunately, these systems show poor rehydrogenation properties and often need catalysts to react in a reasonable temperature-pressure regime.

Zintl phase hydrides can either incorporate hydrogen on interstitial sites or covalently bound to the polyanion (review: [13]), thus showing features of ionic as well as complex hydrides. Furthermore, both bonding schemes can appear next to each other and might help to overcome the problems mentioned above. Additionally, they allow the use of light and inexpensive elements like calcium, potassium, aluminium, silicon, etc. Since Zintl phase hydrides features both, saltlike and complex hydride moieties, decomposition occurs usually at moderate temperatures, e.g. 414 K for $KSiH_3$ [3] and 523 K for $CaSiH_{1.3}$[1] at 0.1 MPa, and show good reversibility.

In situ diffraction has proven to be a valuable tool to study such solid-state gas reactions (recent reviews: [14] for neutron, [15] for X-ray diffraction.) To investigate the incorporation of hydrogen into crystalline structures the use of neutron radiation is often mandatory to localize hydrogen (or more often deuterium) positions. There are several examples demonstrating the benefit of such studies. *In situ* diffraction of the reaction of $Li_3N + H_2 = LiNH_2 + 2\ LiH$, which is an example of a hydrogen storage system due to its reversibility, showed quite different reaction paths depending on the temperature-pressure conditions.[16, 17] Previous studies on the reaction of Zintl phases with hydrogen revealed that reactions happen in one step forming line phases [18, 19] or show intermediate phases with large homogeneity ranges regarding hydrogen [20].

The $AeTt$-H_2 (Ae=Ca-Ba, Tt=Si-Sn) systems show hydrogen rich phases incorporating ionic hydride anions as well as hydrogen covalently bound to the *Tt* polyanions. [2, 21,22] For the SrGe-H_2 system it was shown that the breaking of covalent Ge-H bonds is accompanied by a release of ionic hydrogen from interstitial sites. [20, 23]

This contribution extends the mechanistic understanding of hydrogen uptake and release of Zintl phases using *in situ* thermal analysis and diffraction. We use the heavy element representatives of the *AeTt* system, i.e. BaGe and BaSn, since they show better reactivity than the silicides. Three new, hydrogen poor compounds ($y < 1$) are described that are intermediates in the formation and decomposition of the hydrogen rich phases $BaTtH_y$, $1 < y < 2$.

Experimental

Synthesis

All preparations were done in an argon filled glove box (< 1 ppm H_2O, O_2).
The Zintl phases BaGe and BaSn were prepared from the elements (Ba: rod, 99.3% (ca. 0.7% Sr); Ge: ChemPur, 99.9999%; Sn: powder, ChemPur, 99+%). Stoichiometric mixtures of barium and germanium or barium and tin were sealed inside a niobium (BaGe) or stainless steel (BaSn) metal jacket, which was heated under primary vacuum (0.1 Pa, active pumping). BaGe was melted at 1373 K and subsequently annealed at 1173 K for 40 h. BaSn was annealed at 1273 K for 48 h, then ground and annealed at 1273 K for 48 h again.

Thermal analysis

Differential scanning calorimetry was done *in situ* under hydrogen pressure (H_2-DSC). Measurements were performed with a Q1000 DSC (TA Instruments) equipped with a gas pressure chamber. Aluminum crucibles were filled with about 15-20 mg of the Zintl phase and crimped within a glovebox. Thus, the container was tight against air but still allows hydrogen to penetrate. Samples were placed in the pressure chamber, which was then flushed with hydrogen (Air Liquide, 99.9%) for three times before it was set to the desired starting pressure. Due to isocore set up, the pressure increased during a measurement as shown in the corresponding figures. Samples were heated at a rate of 10 K min^{-1} to a maximum temperature of 700 K. The temperature was usually held for 10 min. In subsequent runs, lower maximum temperatures were used depending on the occurring signals. The heating was then stopped right after a reaction step, and the temperature was held there for 10 min before cooling to room temperature and *ex situ* XRPD characterisation.

Laboratory X-ray powder diffraction (XRPD)

Ex situ XRPD was done using monochromatic Cu-$K_{\alpha1}$-radiation either on a Huber G670 Guinier diffractometer with image plate detector or on a Stoe Stadi P Debye-Scherrer diffractometer with Mythen 1K detector.

In situ synchrotron powder diffraction (*in situ* SPD)

SPD was done at KMC-2 beamline [24] of BESSY II at Helmholtz-Zentrum Berlin (HZB), Germany, using radiation with λ = 118.08(2) pm (10.5 keV). For *in situ* measurements 0.3 mm fused silica capillaries were used, glued into ¼ in VCR-fittings using two component epoxy glue, and attached to a gas handling system (H_2: 99.999%). Heating was realised using a hot air jet. As sample rotation was not yet possible, the resulting poor crystallite statistics allowed qualitative evaluation of the reaction only.

In situ neutron powder diffraction (*in situ* NPD)

In situ NPD was done at the high intensity D20 instrument [25] at the Institut Laue Langevin (ILL), Grenoble, France. Measurements were done at λ = 186.819(3) pm, which was calibrated by an external silicon NIST640b standard sample in a 5 mm vanadium container. *In situ* experiments were done in (leuco-)sapphire single-crystal cells with 6 mm inner diameter, which were connected to a gas supply system (for more details, see [23, 26]). Due to the single-crystalline character of the cell a proper orientation leads to almost no background contribution of the container. For the *in situ* investigations, the sapphire cell was filled with the Zintl phase within a glove box. After attaching to the gas supply system on the diffractometer the reaction chamber was pressurized with D_2 (Air Liquide, 99.8% isotope purity) at ambient temperature. Heating was realized using two laser beams.

All data sets obtained on the ILL D20 instrument are presented with an additional label according to internal raw data labelling (NUMOR labelling). Data refer to proposal 5-22-734 [27].

Rietveld refinement and crystal structure pictures

Crystal structures were Rietveld refined [28, 29] using *FULLPROF* [30,31] (BaSn-D_2 experimentes) or TOPAS [32] (BaGe-D_2 experiments). *In situ* data set were evaluated in sequential refinements. Structure pictures were prepared by *VESTA* [33, 34]. Structural data were normalized using *STRUCTURE TIDY* [35] as implemented in *VESTA*.

Results and Discussion

Preliminary Considerations

The *AeTt* Zintl-phase family (*Ae* = alkaline earth metal, *Tt* = tetrel / group 14 element) shows a rich hydogenation chemistry. For the SrGe-H_2 system three hydride phases are known already. There are hydrogen rich γ-SrGeH_y, 1.10 < y < 1.23, [20, 21, 23] as well as two hydrogen poor phases α-SrGeH_y, y < 0.3 and β-SrGeH_y, that shows a homogeneity range of at least 0.47 < y < 0.75.[20,23]

The Zintl phases *AeTt*, *Ae* = Ca-Ba *Tt*= Si-Pb, crystallize in CrB-structure type (space group type *Cmcm*, No. 63). According to the Zintl-Klemm concept we suspect two-binding Si^{2-}-ions, which form $^1_\infty[Si^{2-}]$-zigzag chains. Alkaline earth metal atoms form sheets of connected Ae_4 tetrahedra that are compressed along the crystallographic *b* direction.

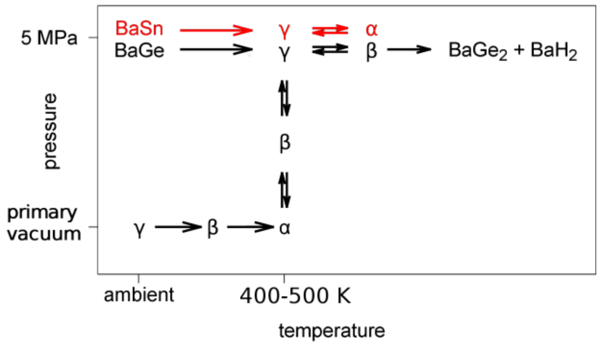

Fig. 1. Reaction scheme for the hydrogenation of BaGe (black) and BaSn (red) showing irreversible and reversible formation steps. Approximate compositions are α-Ba*Tt*H_y (0 < y < 0.36), β-$BaGeH_y$ (y = 0.5) and γ-Ba*Tt*H_y (1 < y < 1.67), (*Tt* = Ge or Sn, no β-$BaSnH_y$ obtained).

Upon formation of α- and β-phases with less than one equivalent hydrogen per formula unit, tetrahedral Ae_4-voids are occupied and the Tt^{2-} polyanions are partially oxidized. As DFT calculations of the hydrogen free phases have shown, there are already partially filled (oxidized) π*-bands at the Fermi edge [36, 37, 38], due to *Tt*-p-*Ae*-d interaction. Upon incorporation of hydrogen these bands are further oxidized increasing bond strength within the zigzag chain and shortening the bond lengths [20, 21, 22]. A similar effect was described for the solid solutions $CaGa_xTt_{1-x}$ (*Tt* = Si (x ≤ 0.6), Sn (x ≤ 0.4)) [39] where electron poor Zintl phases are formed since gallium ions formally have only 5 valence electrons instead of 6. Replacing the alkaline earth metal by an alkaline metal in *AeTt* has a similar effect as partial oxidation by hydrogen. Thus, a bond length shortening within the chain was found in $Na_{0.14}Sr_{0.86}Ge$. [40]

Thermal analysis (see below) of the reaction of BaGe and BaSn with gaseous hydrogen suggests the occurrence of similar hydrogen poor phases as obtained for the SrGe-H_2 system, i.e. α-$BaGeH_y$ and α-$BaSnH_y$ (y < 0.4) and β-$BaGeH_y$ (y = 0.5). Therefore, the recently described phases $BaGeH_{5/3-x}$ [22] and $BaSnH_{4/3-x}$ [21] will be called γ-$BaGeH_y$ and γ-$BaSnH_y$, respectively. α- and β-phases are typical decomposition products at high temperatures. γ-phases release hydrogen under vacuum conditions as well as under hydrogen pressure forming the hydrogen poor phases. Fig. 1 gives a schematic overview of the conditions were the different phases are obtained. Before the reactions are discussed as determined by *in situ* thermal analysis and diffraction, the structures of the new compounds will be discussed in detail.

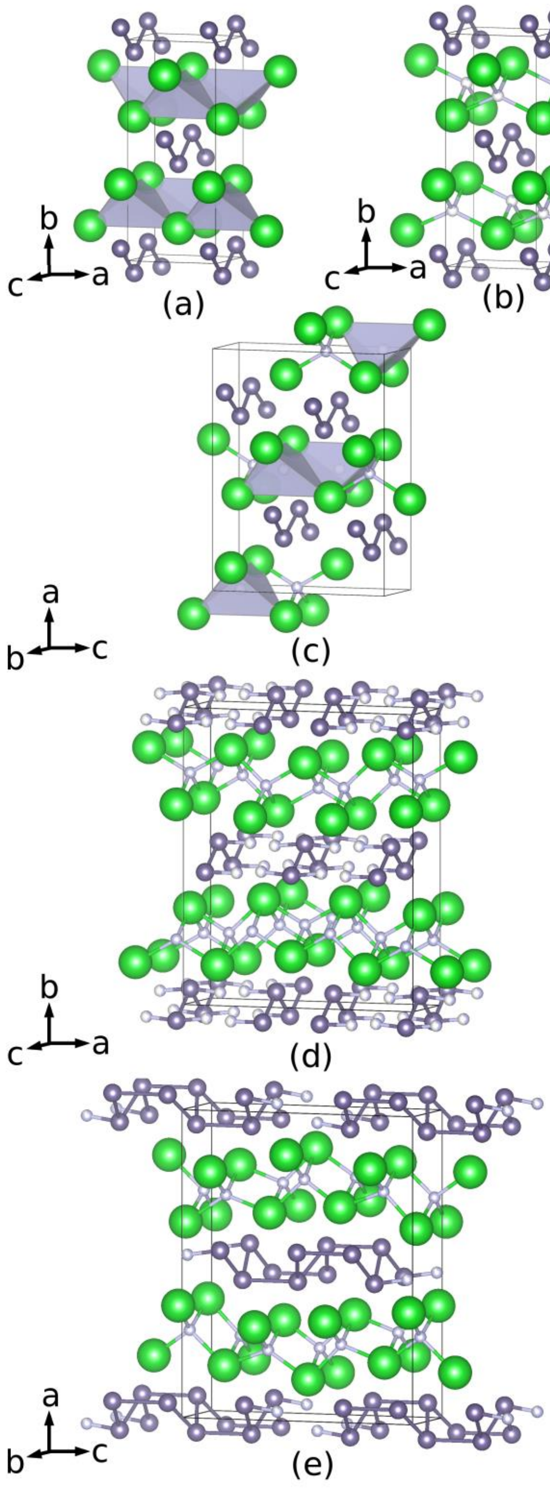

Fig. 2. Crystal structures of **(a)** BaGe / BaSn (*Cmcm*), **(b)** α-$BaGeD_y$ / α-$BaSnD_y$ (*Cmcm*), **(c)** β-$BaGeD_y$ (*Pnma*, $a' = b$, $b' = c$, $c' = 2a$; (1/4, 1/4, 0)), **(d)** γ-$BaGeD_y$ (averaged *Cmcm*-model, the germanium binding D sites are about half occupied (see [22], $a' = 3a$) and **(e)** γ-$BaSnD_y$ (*Pnma*, $a' = b$, $b' = c$, $c' = 3a$). Grey tetrahedra show voids of the hydrogen free Zintl phase and the almost empty deuterium site (D2, SOF = 0.05(3), see Tab 4) of β-$BaGeD_y$. Space groups are given in regard to the parent Zintl phase. Large, green spheres: Ba; medium, grey spheres: Ge / Sn; small white spheres: H/D.

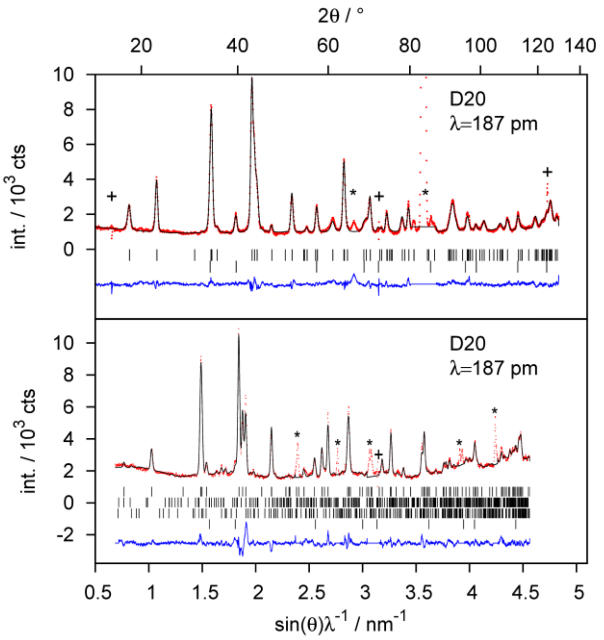

Fig. 3. Rietveld refinement of the crystal structures of **(top)** α-$BaGeD_{0.131(5)}$ (*Cmcm*, *a* = 503.09(3) pm, *b* = 1221.5(2) pm, *c* = 427.38(4) pm; 325(6) K, primary vacuum; Bragg-marker from top: α-$BaGeD_{0.13}$, BaO (6 wt-%); R_{wp} = 6.9%, R_p = 4.9%, *S* =2.7) and **(bottom)** α-$BaSnD_{0.188(4)}$ (*Cmcm*, *a* = 522.72(6) pm, *b* = 1293.6(2) pm, *c* = 463.97(6) pm;478(5) K, 5.2(1) MPa D_2 pressure; Bragg-marker from top: α-$BaSnD_{0.19}$, γ-$BaSnD_{1.3}$ (2 wt-%), Ba_3Sn_5 (4 wt-%), BaO (1 wt-%); R_{wp} = 5.5%, R_p = 4.2%, *S* =2.7). Diffraction data are taken from the *in situ* experiment, thus some reflections of the sapphire cell (*) are present. Defect detector cells are marked with (+).

Crystal structures of α-$BaGeD_y$, α-$BaSnD_y$ and β-$BaGeD_y$, y < 1.0

Using *in situ* neutron diffraction data the crystal structures (see Fig. 2) of the deuterides α-$BaGeD_y$, α-$BaSnD_y$ and β-$BaGeD_y$, y < 1.0 were determined and refined [41].

The crystal structures of the α-phases of the Ba*Tt*-H_2 system (*Tt* = Ge, Sn) were Rietveld refined using a model isotypic to α-$SrGeH_y$ (Fig. 3 and S3; Tab 1, 2 and S3). Due to technical issues (see description of the *in situ* experiment below) the refinement of α-$BaSnD_y$ shows some misfits. The crystal structure of the parent Zintl phases is preserved, but especially lattice parameter *b* is elongated when tetrahedral Ba_4-voids are partially filled with hydrogen.

They appear as decomposition products of the more hydrogen rich β- and γ-$BaGeH_y$ or γ-$BaSnH_y$ under reduced pressure or at high temperatures (Fig. 1). Depending on preparation conditions, the deuterium content is variable indicating a homogeneity range. α-$BaGeD_{0.131(5)}$ was formed from γ-$BaGeD_y$ under vacuum (ca. 10 Pa) and a maximum temperature of 450(2) K. It was recovered at room temperature. Heating β-$BaGeD_y$ for at least 30 min at the same pressure and 502(2) K leads to α-$BaGeD_{0.095(7)}$. γ-$BaSnD_y$ decomposes at ca. 430 K and 5.0(1) MPa D_2 (*in situ* diffraction, see below) into α-$BaSnD_{0.188(4)}$ or at ca.

450 K and 5.5(1) MPa H_2 (H_2-DSC, see below). This phase was not recovered at room temperature since a reversible formation of γ-$BaSnD_y$ occured upon cooling under 5 MPa D_2 at ca. 425 K.

Within the whole *AeTt*-H_2 system, lattice parameter *c* regarding the CrB-type Zintl phases (direction of the zigzag chains) is hardly affected by the hydrogenation. The other lattice parameters strongly change. Therefore, the *b/c*-ratio is a good measure for a structural change. Hydrogen free BaGe shows *b/c* = 2.78-2.79 depending on the temperature. This value increases to 2.83 and finally to 2.86 with increasing hydrogen content of the α-phase (Tab. 3). The *b*/*c*-ratio increases from 2.69 in hydrogen free BaSn to 2.79 in α-$BaSnD_{0.188(4)}$. Thus, it is a proper measure for the hydrogen incorporation in low concentrations.

Table 1. Structural data of the α-phase $BaGeD_{0.131(5)}$, 325(6) K, sapphire cell, primary vacuum (10 Pa), *Cmcm*, *a* = 503.09(3) pm, *b* = 1221.5(2) pm, *c* = 427.38(4) pm, d(Ge-Ge) = 261.6(6) pm, ∢(Ge-Ge-Ge) = 109.5(3)°. Structural data of α-$BaGeD_{0.095(7)}$ are given in Tab. S3.

atom	*x*	*y*	*z*	B_{iso} / 10^4 pm^2	SOF
Ba	0	0.3578(3)	¼	0.62(13)	
Ge	0	0.0618(4)	¼	1.80(10)	
D	0	0.767(3)	¼	0.7(8)	0.131(5)

Table 2. Structural data of the α-phase $BaSnD_{0.188(4)}$, 478(5) K, sapphire cell, 5.2(1) MPa D_2 pressure, *Cmcm*, *a* = 522.72(6) pm, *b* = 1293.60(15) pm, *c* = 463.97(6) pm, d(Sn-Sn) = 294.0(3) pm, ∢(Sn-Sn-Sn) = 104.2(3)°.

atom	*x*	*y*	*z*	B_{iso} / 10^4 pm^2	SOF
Ba	0	0.3530(3)	¼	3.58(6) [a]	
Sn	0	0.0698(3)	¼	3.58 [a]	
D	0	0.7531(12)	¼	4.58 [a]	0.188(4)

[a]Due to similar molar mass (Ba and Sn) and some problems with adjustment of the single crystal cell, constraints were set to B_{iso}(Ba) = B_{iso}(Sn) = B_{iso}(D)-offset; offset = 1.0. Varying the offset did not change the SOF(D) significantly (offset = 0.0 to 2.0: 2 e.s.u. variation, offset = 3.0: 3 e.s.u.)

Table 3. Lattice parameters of the parent Zintl phases, α- and β-Ba*Tt*D_y (*Tt* = Ge, Sn) determined by neutron powder diffraction.

Phase[a]	y	*T* / K	*a* / pm	*b* / pm	*c* / pm	*b/c*	d(*Tt*-*Tt*) / pm
BaGe		298(2)	506.58(2)	1195.5(2)	430.27(2)	2.78	267.6(4)
BaGe		502(2)	507.50(4)	1206.0(2)	431.65(4)	2.79	269.5(4)
α-$BaGeD_y$	0.095(7)	502(2)	505.66(4)	1218.0(2)	429.85(4)	2.83	266.5(6)
α-$BaGeD_y$[b]	0.131(5)	325(6)	503.09(3)	1221.5(2)	427.38(4)	2.86	261.6(6)
β-$BaGeD_y$[c]	0.488(11)	502(2)	1/2*c*' = 495.77(4)	*a*' = 1319.5(2)	*b*' = 421.46(2)	*a*'/*b*' = 3.13	257.1(7)
BaSn		298(2)	532.79(5)	1251.10(10)	465.89(4)	2.69	301.0(5)
α-$BaSnD_y$	0.188(4)	478(5)	522.72(6)	1293.6(2)	463.97(6)	2.79	294.0(3)

[a] All phases crystallize in spacegroup *Cmcm*, exept β-$BaGeH_y$ which cystallizes in space group type *Pnma*;[b] dehydrogenated at T_{max} = 450(2) K;[c] axes reordered and normalised with respect to the CrB-structure type to gain comparability.

The Ge-Ge distance of BaGe was evaluated as 267.6(4) pm (298(2) K) and 269.5(4) pm (502(2) K). The angle within the zigzag chain is 106.4(2)° or 107.0(2)° respectively. BaSn shows a Sn-Sn distance of 301.0(5) pm and a chain angle of 101.4(3)° (298(2) K). Upon formation of the α-phases, the chains are partially oxidized (e.g. $Ge^{2-} + {}^{y}/_{2}\ H_2 \rightarrow Ge^{(2-y)-} + y\ H^-$). Thus, a shortening of the bond lengths is observed. The change in BaGe is small with d(Ge-Ge) = 261.6(6) pm for α-$BaGeD_{0.131(5)}$ at 325(6) K and 266.5(6) pm for α-$BaGeD_{0.095(7)}$ at 502(2) K. The corresponding chain angles are 109.5(3)° and 107.5(3)°, respectively. The formal germanium-electron count of α-$BaGeD_{0.131(5)}$ is comparable to $Na_{0.14}Sr_{0.86}Ge$, which shows a similar bond length d(Ge-Ge) = 260.2(3) pm (293 K) [40]. The shortening of the Sn-Sn bond length is similar and reaches d(Sn-Sn) = 294.0(3) pm (478(5) K). The chain angle increases to 104.2(3)°. The data are summarized in Tab. 3. Ba-D distances are slightly larger than in binary BaH_2 (262 pm [42]) with 261(3)-279(3) pm in α-$BaGeD_{0.095(7)}$ and 269.5(9)-291.6(8) pm in α-$BaSnD_{0.188(4)}$.

While the α-phases show a statistical occupation of tetrahedral voids, the β-phases show hydrogen ordering. For β-$SrGeH_y$ a 2x2-fold superstructure regarding the parent Zintl phase was found.[20] Due to data quality only a preliminary structure model was presented. β-$BaGeH_y$ shows a twofold superstructure along crystallographic *a* direction regarding the parent Zintl phase. The structure was determined with the aid of group-subgroup relations [43]. To reach a doubling of lattice parameter *a* staying in orthorhombic crystal system at least two transitions of type *k2* (klassengleiche transition of index two) are necessary. These symmetry reductions lead to seven space group type candidates. Four of them describe all superstructure reflections according profile fitting. Only one structure model led to an ordered deuterium site occupation. Thus, the structure is described in space group type *Pnma* (*a*'= *b*, *b*'= *c*, *c*' = 2*a*). The symmetry reduction leads to two independent crystallographic sites within Ba_4-tetrahedra as possible deuterium positions. Rietveld refinement (Fig. 4, Tab. 4) of the crystal structure of β-$BaGeD_y$ results in one site (D1, Tab. 4) with 92.5(13)% occupation and one nearly empty site (D2, Tab. 4) with 5.0(10)% occupation giving an approximate composition of β-$BaGeD_{0.5}$.

The filled tetrahedra are more regular than the nearly empty ones with typical Ba-D distances of 254.1(9) pm to 266(2) pm. These values are comparable to the binary hydride BaH_2 with 262 pm on average [42] and they are 5-10% smaller than in the α-phases. The irregular, hardly filled tetrahedral voids show one strongly elongated Ba-D distance longer than 300 pm and a strongly opened Ba-Ba edge.

While the effect on the interchain distances of the α-phases is small, the shortening of the Ge-Ge distance in β-$BaGeH_{0.5}$ from 267.6(4) pm in BaGe to 257.1(7) pm in the hydride is much stronger. The bond length compares well to Li_4Ge_2H, which shows Ge-Ge zigzag chains as well with a Ge-Ge distance of 253 pm [44, 45]. Both examples can be described as Zintl phases with formally $Ge^{1.5-}$-polyanions, which are oxidized in regard to the assumed

Ge^{2-} of a zigzag chain according to the Zintl concept. Thus, the shortened bond lengths correspond to an increased π-bonding due to a depopulation of π*-bands upon hydrogenation.

Thermal analysis

In situ thermal analysis under hydrogen pressure (H_2-DSC) was conducted under several pressure conditions to investigate the reactions of BaGe and BaSn with hydrogen. The hydrogenation of BaGe shows the first strong exothermic signal above 373 K (Fig. 5). Between 3 to 5 MPa starting pressure the signal does not significantly shift, but since it is broad the onset is not well defined. According to *in situ* diffraction (see below) and *ex situ* characterisation, this effect corresponds to the formation of γ-$BaGeH_y$. The partially formation of the β-phase already takes place at room temperature (see below, *in situ* NPD) but does not give any DSC signal. Since the reaction is quite slow and a heating range of 10 K min^{-1} was applied, the exothermic signal might mainly show the direct reaction of BaGe + y/2 H_2 → γ-$BaGeH_y$. Subsequent cycles (T_{max} = 475 K) did not result in further signals.

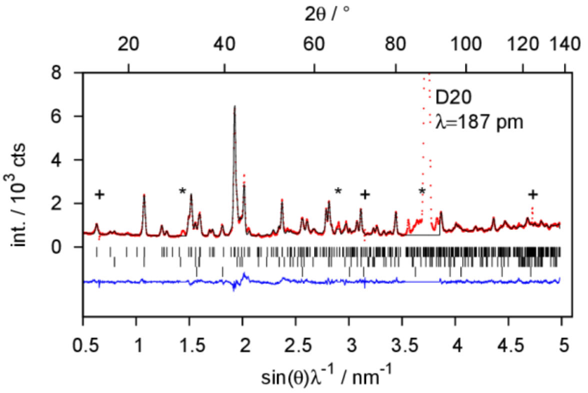

Fig. 4. Rietveld refinement of the crystal structure of β-$BaGeD_{0.488(12)}$ (*Pnma*, *a* = 1319.5(2) pm, *b* = 421.46(2) pm, *c* = 991.54(7) pm; 502(2) K, 0.20(5) MPa D_2; Bragg-marker from top: β-$BaGeD_{0.49}$, α-$BaGeD_{0.22}$ (25 wt-%), BaO (6 wt-%); R_{wp} = 6.9%, R_p = 4.9%, *S* = 2.7) Diffraction data are taken from the *in situ* experiment, thus some reflections of the sapphire cell (*) are present. Defect detector cells are marked with (+).

Table 4. Structural data of the β-phase $BaGeD_{0.488(12)}$, 502(2) K, sapphire cell, 0.20(5) MPa D_2 pressure, *Pnma*, *a* = 1319.5(2) pm, *b* = 421.46(2) pm, *c* = 991.54(7) pm, d(Ge1-Ge2) = 257.1(7) pm, ∢(Ge1-Ge2-Ge1) = 110.1(5)°.

atom	*x*	*y*	*z*	B_{iso} / 10^4 pm^2	SOF
Ba1	0.1050(7)	¼	0.1471(13)	0.8(2)	
Ba2	0.1040(9)	¼	0.6095(17)	B_{iso}(Ba1)	
Ge1	0.3237(6)	¼	0.3893(9)	1.7(2)	
Ge2	0.2820(6)	¼	0.8758(10)	B_{iso}(Ge1)	
D1	0.0031(7)	¼	0.3768(11)	0.7(3)	0.925(13)
D2[a]	x(D1)+½	¾	z(D1)	B_{iso}(D1)	0.050(10)

[a] symmetry condition as inherited from the original super group to fix this nearly empty site within the tetrahedral void.

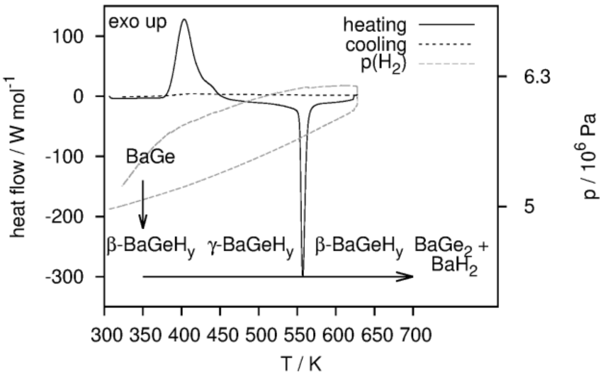

Fig. 5. *In situ* thermal analysis (H_2-DSC) of the hydrogenation of BaGe.

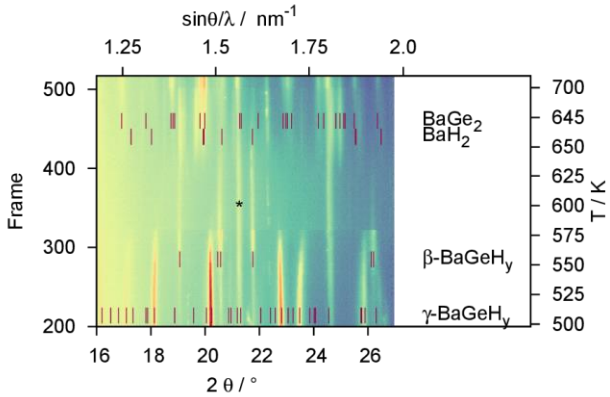

Fig. 6. 2D plot of *in situ* synchrotron powder diffraction (*in situ* SPD) of the hydrogenation of BaGe showing the high temperature region at 5 MPa H_2 and 2K min^{-1} heating rate (20s / frame data collection). (*) marks BaO.

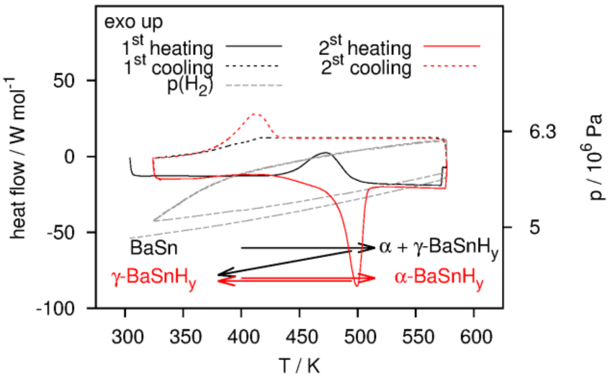

Fig. 7. *In situ* thermal analysis (H_2-DSC) of the hydrogenation of BaSn. A measurement starting directly from γ-$BaSnH_y$ reproduces run two (Fig. S5).

At 553 K and 5.7 MPa H_2 pressure an endothermic decomposition step occurs. With decreasing hydrogen pressure it shifts to 523 K at 3.4 MPa. From *ex situ* characterisation the decomposition product is not clear. Either γ-$BaGeH_y$ (although a reversible DSC signal could never be obtained) or a poorly crystalline product was present. Further heating at elevated pressures leads to the formation of BaH_2 and $BaGe_2$ as seen for the SrGe-H2 system before [20]. *In situ* synchrotron diffraction showed that β-$BaGeH_y$

is formed and subsequently the decomposition in the germanium rich phase and binary hydride takes place (Fig 6). At pressures below 3 MPa H_2 γ-$BaGeH_y$ was not formed from BaGe.

H_2-DSC experiments of the hydrogenation of BaSn give different signals in the first cycle compared to the subsequent ones (Fig. 7). The first run at 5.0 MPa starting pressure shows an exothermic signal at 470 K. Upon cooling no further signal is observed. Subsequent cycles show an endothermic signal at 500 K which was not observed during the first run. A corresponding exothermic signal at 410 K is obtained upon cooling. *Ex situ* characterised samples after one cycle show a mixture of α- and γ-$BaSnH_y$. After the second and subsequent cycles γ-$BaSnH_y$ is the main phase. Using γ-$BaSnH_y$ as starting material for the H_2-DSC experiment, the same patterns as for the second cycle is obtained (Fig. S5). According to *in situ* neutron diffraction (see below), the reversible decomposition step accounts for the formation of α-$BaSnH_y$.

In situ **diffraction**

In situ diffraction experiments were done starting from the CrB-structure type Zintl phases BaGe and BaSn (Rietveld refinement: Fig S1, S2 and S4; Tab. S1, S2 and S4). The deuteration and dedeuteration of BaGe was studied under 5 MPa deuterium pressure and primary vacuum respectively, using neutron diffraction, while the decomposition at high temperatures was studied by synchrotron diffraction at 5 MPa hydrogen pressure. The reversible reaction between α- and β-$BaGeD_y$ was investigated isothermally at 502 K. The reaction of BaSn was observed under 5 MPa isobaric deuterium pressure.

In situ **diffraction of BaGe**

In situ neutron powder diffraction (NPD) of the reaction of BaGe under deuterium pressure and heating was done with 1 min time resolution. A first reaction step already happens at room temperature and low pressures of about 1-2 MPa (Fig. 8). As stated above, this is an effect that was not seen in the H_2-DSC experiment. The obtained phase was indexed in the orthorhombic crystal system (a = 1309.1(13) pm, b = 423.4(3) pm, c = 998.7(8) pm, 298(2) K, 5.1(1) MPa, about 30% phase fraction) and therefore corresponds to β-$BaGeD_y$. The reflections are broad and Rietveld refinement of the structure was not possible. The phase fraction was estimated using the β-$BaGeD_{0.5}$-model described above. Thus, the deuteration reaction could not be evaluated using sequential Rietveld refinement.

After reaching 5 MPa deuterium pressure, isobaric heating was started. The amount of β-$BaGeD_y$ did not increase, but at about 350 K γ-$BaGeD_y$ starts to form, which corresponds to the exothermic DSC signal. In the beginning of this reaction the reflections are broad as well while they sharpen when higher temperatures are reached. The isothermic step at 425 K already shows a total formation of γ-$BaGeD_y$ (except for some BaO impurity). Isobaric heating was stopped at 505 K.

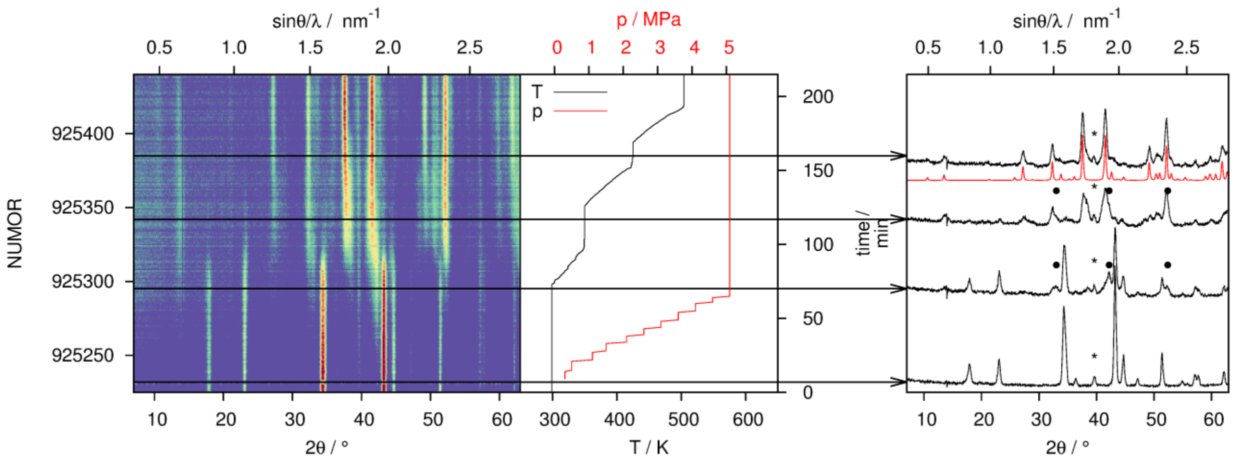

Fig. 8. 2D plot of *in situ* neutron powder diffraction starting with BaGe under D_2 pressure **(left)** as well as selected diffraction patterns **(right)**. The diffraction patterns show BaGe **(bottom)**, the partially formation of β-$BaGeD_y$ (**middle**, marked as a bullet) and the formation of γ-$BaGeH_y$ (**top**, a simulation is given as red curve).(*) marks BaO **(right)**. ILL raw data labelling (NUMOR) is given [27].

The decomposition at 5 MPa hydrogen pressure and high temperatures was observed by *in situ* SPD (Fig. 6). At 580 K a hydrogen poor phase in the orthorhombic crystal system is formed. Metrical relations clearly indicate β-$BaGeH_y$. There is no sign towards the formation of the α-phase. Upon further heating, the phase segregates into the germanium rich Zintl phase $BaGe_2$ and BaH_2 above 650 K.

The *in situ* generated γ-$BaGeD_y$-phase was dedeuterated under primary vakuum (10 Pa), which was studied by *in situ* NPD (Fig. 9). Since crystallinity improved during the first heating cycle, sequential Rietveld refinement was possible. Phase fraction as well as hydrogen content was evaluated. At about 365 K β-$BaGeD_y$ is formed again but is only stable in a small temperature window. Already at 400 K α-$BaGeD_y$ is formed. For the evaluation of γ-$BaGeD_y$ a simplified model with three-fold superstructure (*a' = 3a)* with regard to the hydrogen free Zintl phase BaGe and spacegroup type *Cmcm* was used as described elsewhere (Fig. 2, for more details see Ref. [22] and its Supporting Information). Since there is no evidence for a deuterium release from tetrahedral voids, their occupation was kept fixed at 100%. The occupation of the two about 50% filled chain binding deuterium sites (split position) were constraint to the same value and refined. Fig. 9 shows the sum of these sites which is constant up to 365 K and shows no sign for a homogeneity range. The averaged composition is γ-$BaGeD_y$, y = 1.61(2), which is about the previously published value y = 1.57(3) [22].

The temperature region from 365 K to 425 K is characterised by severe overlap of all three deuteride phases. Therefore, all parameters of γ-$BaGeD_y$ except for the scaling were kept fixed. Nonetheless, deuterium occupations of β-$BaGeD_y$ strongly correlate with the occurrence of α-$BaGeD_y$ and the residual γ-$BaGeD_y$. The occupation of D1 (Tab. 4) goes down a bit, but shows full occupation after γ-$BaGeD_y$ was removed from the sequential refinement. The second tetrahedral void site (D2, Tab. 4) stays empty. Therefore, the varying occupation might be an artefact of the refinement and this phase might show no homogeneity range or only a small one in contrast to β-$SrGeH_y$.[20]

Above 400 K, α-$BaGeD_y$ is formed starting with y = 0.32(3) (*b*/*c* = 2.94, cf. Tab. 3). During the heating process, deuterium is slowly released going down to y = 0.167(10) (*b*/*c* = 2.87, cf. Tab. 3) at the maximum temperature of 450 K. Rietveld refinement after cooling down to 325 K showed a composition α-$BaGeD_{0.131(5)}$.

Under isothermic conditions at 502 K the deuterium pressure was cycled between vacuum (10 Pa) and 0.2 MPa. Diffraction patterns were collected with 10 s time resolution. To improve counting statistics, the experiment was repeated five times and diffraction patterns of equal pressure conditions were summed (Fig. 10). Starting from α-$BaGeD_y$, the β-phase was allowed to form for 2 min at 0.2 MPa to have the same starting conditions for each repetition.

The reaction from β- to α-$BaGeD_y$ is fully reversible and only depends on the applied pressure. On this time scale the occupation of the tetrahedral voids stays constant (Fig. 10). The D1 site of the β-phase shows an occupation of 0.90(4) averaged over the whole experiment except for the points with less than 25 % phase content. The occupation of the empty D2 site was refined as well and shows no additional deuterium incorporation (averaged SOF = 0.029(13)).

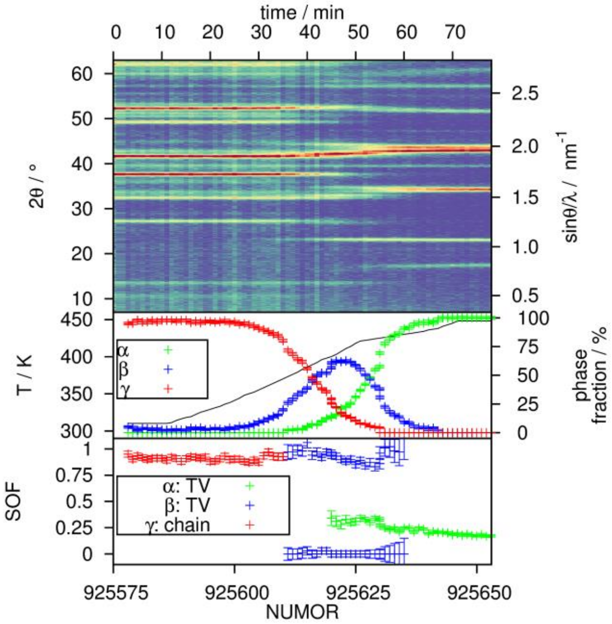

Fig. 9. 2D diffraction plot of the decomposition of *in situ* formed γ-$BaGeD_{1.61}$ under primary vacuum **(top)**, temperature and phase fraction profiles **(middle)** and deuterium site occupation factors (SOF, **bottom**). γ-$BaGeD_y$: sum of the split position of the chain binding sites (chain); α- and β-$BaGeD_y$: tetrahedral voids (TV). ILL raw data labelling (NUMOR) is given [27].

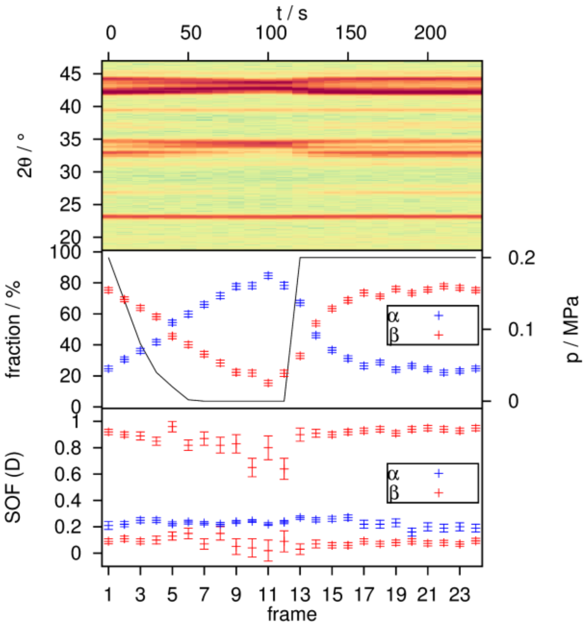

Fig. 10. Pressure dependent cyclic formation of α- (primary vacuum) and β-$BaGeD_y$ (0.2 MPa D_2) at isothermal conditions at 502 K (**top**), pressure and phase fraction profiles (**middle**) and deuterium site occupation factors (SOF) of tetrahedral voids (**bottom**). ILL raw data labelling (NUMOR) is given [27].

α-$BaGeD_y$ shows a constant deuterium occupation on this time scale (averaged SOF = 0.23(2)). A hint pointing towards a phase width is a small volume jump of 0.6% when the sample is pressurized. The *b*/*c* ratio decreases during evacuation from 2.94 to 2.90 and jumps back to 2.95 when the sample is pressurized with deuterium to 0.2 MPa. The volume of β-$BaGeD_y$ is not effected at all (< 0.1% volume change). After a further dehydrogenation under vacuum for 30 min, a composition of α-$BaGeD_{0.095(7)}$ was reached, clearly indicating a homogeneity range of this phase.

In situ neutron diffraction of BaSn

In situ neutron diffraction of BaSn was done under 5.0(1) MPa isobaric deuterium pressure and heating. Diffraction patterns were collected with 1 min time resolution. For serial Rietveld refinement a summation over five frames was applied. The orientation of the single-crystal cell was inadequate and needed correction. Due to this technical issue the experiment was interrupted for about 100 min at elevated temperatures. After the correction some container reflections were still present. Furthermore, a significant fraction of γ-$BaSnD_y$ was already formed. Due to severe overlap with γ-$BaSnD_y$ and the broadness of the reflections the formation of α-$BaSnD_y$ at low temperatures cannot be evaluated unambiguously. Therefore, sequential Rietveld refinement results are shown, starting with the decomposition of γ-$BaSnD_y$ (Fig. 11). At 423 K the decomposition of γ-$BaSnD_y$ starts, which is well below the endothermic DSC signal at 500 K. The reformation of the γ-phase is reversible without hysteresis and the phase fraction starts to increase again after the temperature was below

423 K. The reformation step fits to the exothermic signal obtained in the DSC experiment.

The structure of γ-$BaSnD_y$ was kept fixed during the serial refinement and only the occupation of the tin binding deuterium site was refined. Considering estimated standard uncertainties (e.s.u.). this value stays constant over the whole experiment. The first formation leads to an averaged chemical formula γ-$BaSnD_y$, y = 1.273(13). The reformation during the cooling process results in a slightly larger value of y = 1.291(3). Both evaluations fit the published value y = 1.278(2) [21] reasonably well. Thus, no homogeneity range is assumed here.

Starting with the decomposition of γ-$BaSnD_y$, the α-$BaSnD_y$ is present during the rest of the experiment. The deuterium occupation is sensitive to temperature. It goes down to y = 0.172(4) (*b*/*c* = 2.78) at the highest measured temperature of 519(2) K. Right after the γ-phase started to decompose (430(2) K) about one quarter of the tetrahedral voids is filled (y = 0.260(8); *b*/*c* = 2.80). This value is reached again upon cooling (430(2)K, y = 0.248(4), *b*/*c* = 2.80). After the reformation of γ-$BaSnH_y$, at the end of the *in situ* experiment the α-phase is still present with 31(2) wt-% and reaches a maximum deuterium occupation of y = 0.36(3) (317(2) K, *b*/*c* = 2.81) The formation of a β-phase was not observed.

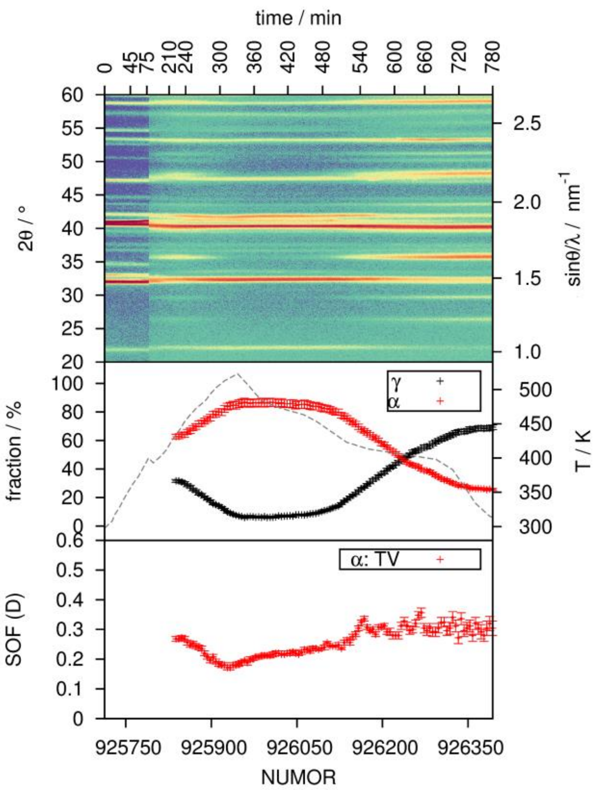

Fig. 11. 2D *in situ* diffraction plot of the reaction of BaSn at 5 MPa D_2 pressure **(top)**, temperature and phase fractions **(middle)** and deuterium site occupation factors (SOF) of tetrahedral voids (TV, **bottom**). SOF(D) of γ-$BaSnD_y$ (chain-binding and TV) are constant (not shown). Due to technical issues (see text) the evaluation starts at *t* = 200 min. ILL raw data labelling (NUMOR) is given [27].

Conclusions

The formation and decomposition of different types of Ba*Tt*H_y-phases, *Tt* = Ge, Sn, were observed by *in situ* diffraction and thermal analysis under several conditions. It could be shown that another two representatives of the system *AeTt*-H_2 show almost reversible hydrogenation properties. Upon decomposition under pressure as well as under vacuum some residual hydrogen stays in tetrahedral voids forming α-Ba*Tt*H_y phases. These show a homogeneity range and a hydrogen occupation sensitive to pressure and temperature. This contribution establishes compositional limits for α-$BaGeH_y$ of at least $0.095(7) \leq y \leq 0.32(3)$ and for α-$BaSnH_y$ of at least $0.172(4) \leq y \leq 0.36(3)$.

The α-phases show slightly shorter *Tt*-*Tt* distances than the hydrogen free phases due to a depopulation of π*-bands and, therefore increased π-bonding within zigzag chains. This correlates well with the electron poor CrB-structure type phase $Na_{0.14}Sr_{0.86}Ge$ [40] or α-$SrGeH_y$, y < 0.3, [20, 23] which have a similar electron count per anion.

Another intermediate phase exists in the BaGe-H_2 system, which can be related to the SrGe-H_2 system [20]. In contrast to β-$SrGeH_y$, β-$BaGeH_{0.5}$ appears to be a line phase with ordered hydrogen occupation. It already appears at room temperature, when BaGe is set under hydrogen pressure and is a decomposition product of γ-$BaGeH_y$ at elevated temperature. Due to stronger oxidation compared to the α-phase, β-$BaGeH_{0.5}$ shows stronger π-bonding and thus decreased Ge-Ge distance. Therefore, the phase can be related to Li_4Ge_2H [44, 45]. Switching between 0.2 MPa D_2 pressure and primary vacuum (10 Pa) at 500 K the formation of α- and β-$BaGeD_y$ can be cycled. At 2 MPa the uptake is fast and α-$BaGeD_y$ reacts almost completely to form β-$BaGeD_{0.5}$ within 1 min. The corresponding deuterium release is slower.

Upon heating to moderate temperatures (< 400 K) and hydrogen pressures above 3 MPa, BaGe and BaSn form hydrogen rich γ-phases as published earlier [21, 22]. These phases are characterised by ionic hydride ions that are incorporated into sheets of tetrahedral Ba_4-voids and hydrogen bound covalently to the polyanion.

The formation of γ-phases can be rationalised using a hypothetical intermediate Ba*Tt*H, where according to the Zintl-Klemm concept Tt^- is supposed to form three-binding polyanions. Due to the rigid hydride filled cationic sheets, the Tt^- atoms cannot solely form bonds to other Tt^- ions but need to additionally form *Tt*-H bonds (see Fig. 2e). Filling tetrahedral voids is thus directly related to the formation of *Tt*-H bonds and vice versa. Since Ge-H and Sn-H bonds are thermally labile, the γ-phases decompose at moderate temperatures under vacuum or 5 MPa hydrogen pressure and need to release additional hydrogen from tetrahedral Ba_4-sites. The decomposition temperatures fit the thermal decomposition of polygermane $(GeH_y)_\infty$ at 470-520 K [46] reasonably well. Therefore these phases show a good (partial) reversibility relating them to classical interstitial hydrides combined with moderate decomposition temperatures due to thermally labile *Tt*-H bonds. In addition to the almost complete reversibility the filling of tetrahedral voids shows fast kinetics as shown by the reaction of α- to β-BaGeH$_y$. This might serve as a starting point for the search of proper hydrogen storage systems within the class of Zintl phases.

Acknowledgements

We thank the Institute Laue-Langevin (ILL) for providing neutron (proposal 5-22-734) and the Helmholtz Zentrum Berlin (HZB) for providing synchrotron beam time (proposal 15202481). Furthermore, we want to thank Dr. Dirk Wallacher and Nico Grimm for set up and support with the *in situ* experiment at BESSY II. We thank the Deutsche Forschungsgemeinschaft (DFG, grant Ko1803/8–1) and the Fonds der Chemischen Industrie (Grant 194371) for financial support.

References

[1] M. Aoki, N. Ohba, T. Noritake, S. Towata, Reversible hydriding and dehydriding properties of CaSi: Potential of metal silicides for hydrogen storage, *Appl. Phys. Lett.*, 2004, **85**, 387-388.
[2] N. Ohba, M. Aoki, T. Noritake, K. Miwa, S. Towata, First-principles study of a hydrogen storage material CaSi, *Phys. Rev. B*, 2005, **72**, 075104.
[3] J.-N. Chotard, W. S. Tang, P. Raybaud and R. Janot, Potassium Silanide ($KSiH_3$): A Reversible Hydrogen Storage Material, *Chem. - Eur. J.*,2011, **17**, 12302-12309.
[4] J. Zhang, S. Yan, H. Qu, X. Yu, P. Peng, Alkali metal silanides α-MSiH3: A family of complex hydrides for solid-state hydrogen storage, *Int. J. Hydrogen Energy*, 2017, **42**, 12405-12413.
[5] F. Gingl, T. Vogt, E. Akiba, Trigonal $SrAl_2H_2$: the first Zintl phase hydride, *J. Alloys Compd.*, 2000, **306**, 127-132.
[6] Y. Zhu, W. Zhang, Z. Liu, L. Li, Hydrogen storage properties of the Zintl phase alloy $SrAl_2$ doped with TiF_3, *J. Alloys Compd.*, **2010**, *492*, 277-281.
[7] S. Orimo, Y. Nakamori, J. R. Eliseo, A. Züttel, C. M. Jensen, Complex Hydrides for Hydrogen Storage, *Chem. Rev.*, 2007, **107**, 4111-4132.
[8] F.H. Stephens, V. Pons, R. T. Baker, Ammonia-borane: the hydrogen source par excellence?, *Dalton Trans.*, 2007, 2613-2626.
[9] B. Sakintuna, F. Lamari-Darkrim, M. Hirscher, *Int. J. Hydrogen Energy*, 2007, **32**, 1121-1140.
[10] I. Jain, C: Lal, A. Jain, Hydrogen storage in Mg: A most promising material, *Int. J. Hydrogen Energy*, 2010, **35**, 5133-5144.
[11] N. Rusman, M. Dahari, A review on the current progress of metal hydrides material for solid-state hydrogen storage applications, *Int. J. Hydrogen Energy*, 2016, **41**, 12108-12126.
[12] H. Wang, H. Lin, W. Cai, L. Ouyang, M. Zhu, Tuning kinetics and thermodynamics of hydrogen storage in light metal element based systems - A review of recent progress, *J. Alloys Compd.*, 2016, **658**, 280-300.
[13] U. Häussermann, V. F. Kranak, K. Puhakainen, Hydrogenous Zintl Phases: Interstitial Versus Polyanionic Hydrides, *Struct. Bond.*, 2010, **139**, 143-161.
[14] T. C. Hansen, H. Kohlmann, Chemical Reactions followed by in situ Neutron Powder Diffraction, *Z. Anorg. Allg. Chem.*, 2014, **640**, 3044-3063.
[15] K. T. Möller, B. R. S. Hansen, A.-C. Dippel, J.-E. Jørgensen, T. R. Jensen, Characterization of Gas-Solid Reactions using In Situ Powder X-ray Diffraction, *Z. Anorg. Allg. Chem.*, 2014, **640**, 3029-3043.

[16] D. J. Bull, E. Weidner, I. L. Shabalin, M. T. F. Telling, C. M. Jewell, D. H. Gregory, D. K Ross, Pressure-dependent deuterium reaction pathways in the Li-N-D system, *Phys. Chem. Chem. Phys.*, 2010, **12**, 2089-2097.
[17] G. Behrendt, C. Reichert, H. Kohlmann, Hydrogenation Reaction Pathways in the Systems Li_3N-H_2, Li_3N-Mg-H_2, and Li_3N-MgH_2-H_2 by in Situ X-ray Diffraction, in Situ Neutron Diffraction, and in Situ Thermal Analysis, *J. Phys. Chem. C,* 2016, **120**, 13450-13455.
[18] P. Wenderoth, H Kohlmann, In Situ Neutron Powder Diffraction of the Formation of $SrGa_2D_2$, and Hydrogenation Behavior of $YbGa_2$ and $EuGa_2$, *Inorg. Chem.*, 2013, **52**, 10525-10531.
[19] H. Auer, H. Kohlmann, In situ Investigations on the Formation and Decomposition of $KSiH_3$ and $CsSiH_3$, *Z. Anorg. Allg. Chem.*, 2017, **643**, 945-951.
[20] H. Auer, D. Wallacher, T. C. Hansen, H. Kohlmann, In Situ Hydrogenation of the Zintl Phase SrGe, *Inorg. Chem.*, 2017, **56**, 1072-1079.
[21] H. Auer, R. Guehne, M. Bertmer, S. Weber, P. Wenderoth, T. C. Hansen, J. Haase, H. Kohlmann, Hydrides of Alkaline Earth-Tetrel (AeTt) Zintl Phases: Covalent Tt-H Bonds from Silicon to Tin, *Inorg. Chem.*, 2017, **56**, 1061-1071.
[22] H. Auer, R. Schlegel, O. Oeckler, H. Kohlmann, Structural and Electronic Flexibility in Hydrides of Zintl Phases with Tetrel-Hydrogen and Tetrel-Tetrel Bonds, *Angew. Chem., Int. Ed.*, 2017, **56**, 12344-12347; H. Auer, R. Schlegel, O. Oeckler, H. Kohlmann, Strukturelle und elektronische Flexibilität in Hydriden von Zintl-Phasen mit Tetrel-Wasserstoff- und Tetrel-Tetrel-Bindung, *Angew. Chem.*, 2017, **129**, 12515-*12518.*
[23] A. Götze, H. Auer, R. Finger, T. C. Hansen, H. Kohlmann, A sapphire single-crystal cell for in situ neutron powder diffraction of solid-gas reactions, *Phys. B*, 2017, DOI: 10.1016/j.physb.2017.11.024.
[24] Helmholtz-Zentrum Berlin für Materialien und Energie, KMC-2: an X-ray beamline with dedicated diffraction and XAS endstations at BESSY II, *Journal of large-scale research facilities*, 2016, **2**, A49.
[25] T. C. Hansen, P. F. Henry, H. E. Fischer, J. Torregrossa, P. Convert, The D20 instrument at the ILL: a versatile high-intensity two-axis neutron diffractometer, *Meas. Sci. Technol.*, 2008, **19**, *034001.*
[26] H. Kohlmann, N. Kurtzemann, R. Weihrich, T. Hansen, In situ Neutron Powder Diffraction on Intermediate Hydrides of $MgPd_3$ in a Novel Sapphire Gas Pressure Cell, *Z. Anorg. Allg. Chem.*, 2009, **635**, *2399-2405.*
[27] H. Kohlmann, H. Auer, A. Götze, T. Hansen, S. Weber, Reaction pathways to the Zintl phase hydrides CaSiH and $MGeH_x$ (M = Sr, Ba), *Institut Laue-Langevin (ILL)*, 2015, doi:10.5291/ILL-DATA.5-22-734.
[28] H. M. Rietveld, Line profiles of neutron powder-diffraction peaks for structure refinement, *Acta Crystallogr.*, 1967, **22**, 151-152.
[29] H. M. Rietveld, A profile refinement method for nuclear and magnetic structures, *J. Appl. Crystallogr.*, 1969, **2**, 65-71.
[30] J. Rodriguez-Carvajal, Recent advances in magnetic structure determination by neutron powder diffraction, *Phys. B, 1993, **192**, 55 - 69.*
[31] *FullProf.2k*, Version 5.30 - Mar2012-ILL JRC.
[32] Bruker AXS, *TOPAS* version 5, www.bruker-axs.com.
[33] K. Momma & F. Izumi, VESTA3 for three-dimensional visualization of crystal, volumetric and morphology data, *J. Appl. Crystallogr., 2011, **44**, 1272-1276.*
[34] *VESTA* - Visualisation for Electronic and STructural Analysis, version 3.3.1.

[35] L. M. Gelato, E. Parthé, STRUCTURE TIDY - a computer program to standardize crystal structure data, *J. Appl. Crystallogr.*, *1987*, ***20***, *139-143*.
[36] E. C. Reyes, E. D. Stalder, C. Mensing, S. Budnyk, R. Nesper, Unexpected Magnetism in Alkaline Earth Monosilicides, *J. Phys. Chem. C,* 2011, **115**, 1090-1095.
[37] E. C. Reyes, R. Nesper, Electronic Structure and Properties of the Alkaline Earth Monosilicides, *J. Phys. Chem. C,* 2012, **116**, 2536-2542.
[38] I. M. Kurylyshyn, T. F. Fässler, A. Fischer, C. Hauf, G. Eickerling, M. Presnitz, W. Scherer, Probing the Zintl-Klemm Concept: A Combined Experimental and Theoretical Charge Density Study of the Zintl Phase CaSi, *Angew. Chem., Int. Ed.*, 2014, **53**, 3029-3032.
[39] W. Harms, M. Wendorff, C. Röhr, Structure and bonding of ternary gallides $CaGa_{1-x}(Si/Sn/Al/In)_x$ with the CrB type and related structures, *J. Alloys Compd.*, 2009, **469**, 89-101.
[40] Q.-X.Xie, R. Nesper, Crystal structure of sodium strontium monogermanide, $Na_xSr_{1-x}Ge$ (x = 0.14), *Z. Kristallogr. - New Cryst. Struct.*, 2003, **218**, 291-292.
[41] Further details of the crystal structure investigations may be obtained from FIZ Karlsruhe, 76344 Eggenstein-Leopoldshafen, Germany (fax: (+49)7247-808-666; e-mail: crysdata(at)fiz-karlsruhe(dot)de, on quoting the deposition numbers CSD-433794 (α-$BaGeD_{0.09}$), CSD-433795 (α-$BaGeD_{0.13}$), CSD-433796 (α-$BaSnD_{0.19}$), CSD-433797 (β-$BaGeD_{0.49}$).
[42] V. P. Ting, P. F. Henry, H. Kohlmann, C. C. Wilson, M. T. Weller, *Phys. Chem. Chem. Phys.* 2010, **12**, 2083-2088.
[43] H. Bärnighausen, Group-Subgroup realtions between space groups: a useful tool in crystal chemistry, *MATCH: Commun. Math. Comput. Chem.*, 1980, **9**, 139-175.
[44] H. Wu, W. Zhou, T. J. Udovic, J. J. Rush, T. Yildirim, M. R. Hartman, R. C. Bowman, J. J. Vajo, Neutron vibrational spectroscopy and first-principles calculations of the ternary hydrides Li_4Si2H(D) and Li_4Ge_2H(D): Electronic structure and lattice dynamics, *Phys. Rev. B,* 2007, **76**, 224301.
[45] H. Wu, M. R. Hartman, T. J. Udovic, J. J. Rush, W. Zhou, R. C. Bowman Jr, J. J. Vajo, Structure of the novel ternary hydrides Li_4Tt_2D (Tt= Si and Ge), *Acta Crystallogr., Sect. B,* 2007, **63**, 63-68.
[46] E. Bianco, S. Butler, S. Jiang, O. D. Restrepo, W. Windl, J. E. Goldberger, Stability and Exfoliation of Germanane: A Germanium Graphane Analogue, *ACS Nano,* 2013, **7**, 4414-4421.